

Zirconium-Substituted Isopolytungstates: Structural Models for Zirconia-Supported Tungsten Catalysts

Hugo Carabineiro,^{†,‡} Richard Villanneau,^{*,§} Xavier Carrier,^{*,‡} Patrick Herson,[§] Francisco Lemos,[†] Fernando Ramôa Ribeiro,[†] Anna Proust,[§] and Michel Che^{‡,||}

Centro de Engenharia Biológica e Química, Instituto Superior Técnico, Universidade Técnica de Lisboa, Avenida Rovisco Pais, 1049-001 Lisboa, Portugal, Laboratoire de Réactivité de Surface (UMR 7609, CNRS) and Laboratoire de Chimie Inorganique et Matériaux Moléculaires (UMR 7071, CNRS), Université Pierre & Marie Curie, 4 place Jussieu, 75252 Paris Cedex 05, France, and Institut Universitaire de France

Received November 9, 2005

The synthesis and characterization of a series of mixed W–Zr polynuclear Lindqvist-type complexes, deriving from hexatungstate $[W_6O_{19}]^{2-}$, are described in this work. This family of compounds is built from $\{W_5O_{18}Zr\}^{2-}$ moieties as shown by the X-ray structures of the monomeric $[W_5O_{18}Zr(H_2O)_{3-n}(DMSO)_n]^{2-}$ ($n = 1$ and 2) and dimeric $[\{W_5O_{18}Zr(\mu-OH)\}_2]^{6-}$ anions. A comprehensive spectroscopic study (^{183}W NMR, FTIR, Raman, EXAFS, and EPR) of these compounds is presented. The goal of incorporating Zr^{IV} cations into an oxotungstic core is to obtain spectroscopic models that could mimic the interactions that develop in supported catalysts between the active phase and the supporting oxide. This work tends to show that these molecular compounds can be regarded as soluble structural analogues of WO_x/ZrO_2 catalysts, which are interesting candidates for the skeletal isomerization of light n -alkanes.

1. Introduction

Polyoxometalates (POMs) are metal–oxygen anion clusters of well-defined structure¹ whose importance to the field of catalysis has long been recognized.² Because their acidic and redox properties can be highly controlled, POMs are particularly useful in both homogeneous and heterogeneous catalytic applications, accounting for about 80% of their patented applications worldwide.³ Much of the interest in POMs comes from the fact that they resemble fragments of

metal oxides of finite size and shape⁴ and therefore may be regarded as molecular-scale models for metal oxide catalysts.^{5,6}

POMs are used in catalysis either as salts (in their bulk form) or spread on the surface of supports such as silica,⁷ carbon,⁸ and alumina⁹ in order to increase their exposed surface area. Additionally, POMs are also used as catalyst precursors,¹⁰ although their primary structure is often decomposed during the preparation steps. Depending on the

* To whom correspondence should be addressed. E-mail: carrier@ccr.jussieu.fr (X.C.), villaneau@ccr.jussieu.fr (R.V.). Phone: +33 1 44 27 60 05. Fax: +33 1 44 27 60 33.

[†] Universidade Técnica de Lisboa.

[‡] Laboratoire de Réactivité de Surface (UMR 7609, CNRS), Université Pierre & Marie Curie.

[§] Laboratoire de Chimie Inorganique et Matériaux Moléculaires (UMR 7071, CNRS), Université Pierre & Marie Curie.

^{||} Institut Universitaire de France.

- (1) Pope, M. T. *Heteropoly- and Isopolyoxometalates*; Springer-Verlag: Berlin, 1983. Baker, L. C. W.; Glick, D. C. *Chem. Rev.* **1998**, *98*, 3.
- (2) Moffat, J. B. *Metal Oxygen Clusters: The surface and catalytic properties of heteropolyoxometalates*; Kluwer: New York, 2001. Kozhevnikov, I. *Chem. Rev.* **1998**, *98*, 171. Lee, K.-Y.; Misono, M. In *Handbook of Heterogeneous Catalysis*; Knözinger, H., Weitkamp, J., Ertl, G., Eds.; Wiley-VCH: Weinheim, Germany, 1997; Vol. 2, p 119.
- (3) Katsoulis, D. *Chem. Rev.* **1998**, *98*, 359.

(4) Baker, L. C. W. *Advances in the Chemistry of Coordination Compounds*; Macmillan: New York, 1961.

(5) Fournier, M.; Louis, C.; Che, M.; Chaquin, P.; Masure, D. *J. Catal.* **1989**, *119*, 400. Masure, D.; Chaquin, P.; Louis, C.; Che, M.; Fournier, M. *J. Catal.* **1989**, *119*, 415.

(6) Villanneau, R.; Carabineiro, H.; Carrier, X.; Thouvenot, R.; Herson, P.; Lemos, F.; Ramôa Ribeiro, F.; Che, M. *J. Phys. Chem. B* **2004**, *108*, 12465.

(7) Kasztelan, S.; Moffat, J. B. *J. Catal.* **1987**, *106*, 512. Rocchiccioli-Deltcheff, C.; Amirouche, M.; Che, M.; Tatibouët, J.-M.; Fournier, M. *J. Catal.* **1990**, *125*, 292. Vazquez, P.; Pizzio, L.; Caceres, C.; Blanco, M.; Thomas, H.; Alesso, E.; Finkielstein, L.; Lantano, B.; Moltrasio, G.; Aguirre, J. J. *Mol. Catal., A* **2000**, *161*, 223.

(8) Dupont, P.; Védrine, J. C.; Paumard, E.; Hecquet, G.; Lefebvre, F. *Appl. Catal., A* **1995**, *129*, 217. Chimienti, M. E.; Pizzio, L. R.; Caceres, C. V.; Blanco, M. N. *Appl. Catal., A* **2001**, *208*, 7. Lapkin, A.; Bozkaya, B.; Mays, T.; Borello, L.; Edler, K.; Crittenden, B. *Catal. Today* **2003**, *81*, 611.

(9) Sharma, P.; Vyas, S.; Patel, A. *J. Mol. Catal., A* **2004**, *214*, 281.

type of POM and support, the resulting catalyst may contain surface species that range from well-dispersed monometalate moieties to bulk oxides or mixtures thereof. Additionally, POMS of ill-defined structure may also form on the surface of monolayer-type mixed-oxide catalysts as a result of support dissolution.¹¹

Following their early discovery in the late 1980s,¹² many efforts have been conducted in order to understand, on a molecular basis, the structure of the catalytically active WO_x phase in WZ catalysts.^{13–15} These catalysts constitute potential substitutes of environmentally harmful liquid acids and halogenated aluminas for the industrial isomerization of *n*-alkanes.¹⁶ However, detailed characterization of WZ is often difficult because of a lack of molecular-scale spectroscopic techniques that can be successfully applied. For instance, the Raman spectra of WZ catalysts show vibrational features of the ZrO_2 support seriously overlapping those of the WO_x phase in the low-frequency region and, hence, further insight into vibrational modes of the oxotungstic phase is seriously limited.

Owing to the structural analogy between polyoxotungstates and two- or three-dimensional tungsten oxides,⁴ molecular zirconium-substituted isopolytungstates can be envisaged as structural and spectroscopic models of WZ catalysts. Using a similar methodology, Curtis and Druker¹⁷ and more recently Herbst et al.¹⁸ investigated potential analogies between metal sulfide clusters and industrial hydrodesulfurization catalysts. However, these studies focused more on the catalytic behavior rather than on spectroscopic properties.

The incorporation of Zr^{IV} in the polyoxotungstate framework is intended to mimic the tungstic phase–oxide support interaction in WZ catalysts. In this context, the study of Zr^{IV} derivatives of the close-packed Lindqvist $[\text{W}_6\text{O}_{19}]^{2-}$ anion appears to be of interest because it provides stable and well-defined clusters in which the Zr^{IV} and W^{VI} cations are in intimate interaction. After the first single-crystal X-ray characterization of a dimeric Zr^{IV} -substituted isopolytungstate (i.e., the dimeric $[\{\text{W}_5\text{O}_{18}\text{Zr}(\mu\text{-OH})\}_2]^{6-}$) described in a previous work,⁶ we present here a rational description of the formation of $\{\text{W}_5\text{O}_{18}\text{Zr}\}^{2-}$ -containing complexes, including the complete structural and spectroscopic characterization of 7- and 8-fold-coordinated Zr^{IV} derivatives.

2. Experimental Section

2.a. Preparation of the Compounds. 2.a.1. Generalities.

Reagent-grade solvents [acetonitrile, dimethyl ether, and dimethyl sulfoxide (DMSO)] and chemicals [$\text{Na}_2\text{WO}_4 \cdot 2\text{H}_2\text{O}$, tetramethylammonium chloride (Me_4NCl), tetrabutylammonium bromide ($^t\text{Bu}_4\text{NBr}$), tetrabutylammonium hydroxide ($^t\text{Bu}_4\text{NOH}$), and Na_2SO_4] were purchased from Aldrich, ACROS Organics, or Fluka and used as received. $\text{ZrOCl}_2 \cdot 8\text{H}_2\text{O}$ was purchased from ACROS Organics. Elemental analyses were performed by the Service de Microanalyses (Université Pierre et Marie Curie, Paris, France) and the Laboratoire Central d'Analyses du CNRS (Vernaison, France).

2.a.2. Preparation of $[\text{W}_5\text{O}_{18}\text{Zr}(\text{H}_2\text{O})_3]^{2-}$ (1a**).** The Me_4N^+ salt of **1a** was prepared according to the procedure described by Chauveau et al.¹⁹ $\text{ZrOCl}_2 \cdot 8\text{H}_2\text{O}$ (1.289 g, 0.004 mol) was dissolved in 500 mL of a 1 M solution of Na_2SO_4 (71 g) previously acidified to $\text{pH} = 2$ with H_2SO_4 . The resulting solution was then diluted to 800 mL with distilled water (solution A). A second solution was prepared by dissolving 0.02 mol of $\text{Na}_2\text{WO}_4 \cdot 2\text{H}_2\text{O}$ (6.60 g) in 70 mL of distilled water. This solution was then brought to boiling followed by the immediate addition of 8 mL of HCl (5 M, e.g., 0.04 mol) under vigorous stirring. The yellowish solution (due to the decatungstate $[\text{W}_{10}\text{O}_{32}]^{4-}$ anions) was immediately cooled in an ice bath (solution B). The cold solution B was then added dropwise to solution A under stirring, and the resulting solution was allowed to stand at room temperature for 3 days. A total of 4 g of Me_4NCl was then added, leading to slow crystallization of the Me_4N^+ salt of **1a**. Crystals of $(\text{Me}_4\text{N})_2(\mathbf{1a})$ were systematically twinned, preventing X-ray structural determination. A total of 3.32 g of $(\text{Me}_4\text{N})_2(\mathbf{1a})$ was then collected after 2 days, yielding 55% based on Zr. The number of water molecules coordinated to the Zr atom was determined from thermogravimetric analysis–differential thermal analysis (TGA–DTA) measurements. $(\text{Me}_4\text{N})_2(\mathbf{1a})$. Raman: ν 759 (m), 839 (m), 928 (s), 934 (s), 946 (sh), 972 (vs) cm^{-1} . IR (KBr): ν 3030 (w), 1487(m), 963 (s), 945 (s, Me_4N^+ cation), 930 (sh, Me_4N^+ cation), 855 (sh), 815 (br), 685 (m), 665 (sh), 640 (s), 590 (sh), 555 (m), 465 (m), 420 (s), 345 (w) cm^{-1} . Elem anal. Calcd for $\text{C}_8\text{H}_{30}\text{N}_2\text{O}_{21}\text{W}_5\text{Zr}$: C, 6.40; H, 2.00; N, 1.87; W, 61.26; Zr, 6.08. Found: C, 5.84; H, 2.12; N, 1.66; W, 57.87; Zr, 5.78.

2.a.3. Preparation of $[\text{W}_5\text{O}_{18}\text{Zr}(\text{H}_2\text{O})_2(\text{DMSO})]^{2-}$ (1b**).** Complex $(\text{Me}_4\text{N})_2(\mathbf{1a})$ (0.2 g, 0.133 mmol) was dissolved in 20 mL of boiling DMSO. The solution was filtered in order to remove the solute excess. A portion of water (10 mL) was added, and the solution was allowed to stand at room temperature for 2 months, during which time small uncolored cubic crystals were formed. A total of 0.070 g (0.042 mmol) of $(\text{Me}_4\text{N})_2(\mathbf{1b}) \cdot \text{DMSO} \cdot \text{H}_2\text{O}$ was

- (10) Martin, C.; Lamonier, C.; Fournier, M.; Mentré, O.; Harlé, V.; Guillaume, D.; Payen, E. *Inorg. Chem.* **2004**, *43*, 4636.
 (11) Carrier, X.; d'Espinose de la Caillerie, J.-B.; Lambert, J.-F.; Che, M. *J. Am. Chem. Soc.* **1999**, *121*, 3377.
 (12) Hino, M.; Arata, K. *Chem. Commun.* **1987**, 1259.
 (13) Afanasiev, P.; Geantet, C.; Breysse, M.; Coudurier, G.; Védrine, J. C. *J. Chem. Soc., Faraday Trans.* **1994**, *90*, 193. Kim, D. S.; Ostromecki, M.; Wachs, I. E. *J. Mol. Catal., A* **1996**, *106*, 93. Gazzoli, D.; Valigi, M.; Dragone, R.; Marucci, A.; Mattei, G. *J. Phys. Chem. B* **1997**, *101*, 11129. Santiesteban, J. G.; Vartuli, J. C.; Han, S.; Bastian, R. D.; Chang, C. D. *J. Catal.* **1997**, *168*, 431. Yoshinaga, Y.; Kudo, M.; Hasegawa, S.; Okuhara, I. T. *Appl. Surf. Sci.* **1997**, *121/122*, 339. Ji, W.; Hu, J.; Chen, Y. *Catal. Lett.* **1998**, *53*, 15. Barton, D. G.; Shtein, M.; Wilson, R. D.; Soled, S. L.; Iglesia, E. *J. Phys. Chem. B* **1999**, *103*, 630. Barton, D. G.; Soled, S. L.; Meitzner, G. D.; Fuentes, G. A.; Iglesia, E. *J. Catal.* **1999**, *181*, 57. Naito, N.; Katada, N.; Niwa, M. *J. Phys. Chem. B* **1999**, *103*, 7206. Vartuli, J. C.; Santiesteban, J. G.; Traverso, P.; Cardona-Martínez, N.; Chang, C. D.; Stevenson, S. A. *J. Catal.* **1999**, *187*, 131. Baertsch, C. D.; Wilson, R. D.; Barton, D. G.; Soled, S. L.; Iglesia, E. *Stud. Surf. Sci. Catal.* **2000**, *130*, 3225. Punnoose, A.; Seehra, M. S.; Wender, I. *Fuel Proc. Technol.* **2001**, *74*, 33. Hadjiivanov, K.; Lukinskas, P.; Knözinger, H. *Catal. Lett.* **2002**, *82*, 73. Punnoose, A.; Seehra, M. S. *Catal. Lett.* **2002**, *78*, 157. Valigi, M.; Gazzoli, D.; Pettiti, I.; Mattei, G.; Colonna, S.; Rossi, S. D.; Ferraris, G. *Appl. Catal., A* **2002**, *231*, 159. Kuba, S.; Lukinskas, P.; Grasselli, R. K.; Gates, B. C.; Knözinger, H. *J. Catal.* **2003**, *216*, 353. Triwahyono, S.; Yamada, T.; Hattori, H. *Appl. Catal., A* **2003**, *250*, 65. Onfroy, T.; Clet, G.; Houalla, M. *J. Phys. Chem. B* **2005**, *109*, 3345. Carrier, X.; Lukinskas, P.; Kuba, S.; Stievano, L.; Wagner, F. E.; Che, M.; Knözinger, H. *ChemPhysChem* **2004**, *5*, 1. Kuba, S.; Che, M.; Grasselli, R. K.; Knözinger, H. *J. Phys. Chem. B* **2003**, *107*, 3459.
 (14) Scheithauer, M.; Grasselli, R. K.; Knözinger, H. *Langmuir* **1998**, *14*, 3019. Scheithauer, M.; Cheung, T.-K.; Jentoft, R. E.; Grasselli, R. K.; Gates, B. C.; Knözinger, H. *J. Catal.* **1998**, *180*, 1.
 (15) Kuba, S.; Heydorn, P. C.; Grasselli, R. K.; Gates, B. C.; Che, M.; Knözinger, H. *Phys. Chem. Chem. Phys.* **2001**, *3*, 146.
 (16) Ono, Y. *Catal. Today* **2003**, *81*, 3.
 (17) Curtis, M. D.; Druker, S. H. *J. Am. Ceram. Soc.* **1997**, *119*, 1027.
 (18) Herbst, K.; Monari, M.; Brorson, M. *Inorg. Chem.* **2002**, *41*, 1336.

- (19) Chauveau, F.; Éberlé, J.; Lefebvre, J. *Nouv. J. Chim.* **1985**, *9*, 315.

then collected (32% yield). $(\text{Me}_4\text{N})_2(\mathbf{1b})\cdot\text{DMSO}\cdot\text{H}_2\text{O}$. Raman: ν 670 (w), 688 (m), 721 (w), 757 (m), 833 (m), 923 (s), 938 (m), 967 (vs), 994 (w) cm^{-1} . IR (KBr): ν 3030 (w), 1487 (m), 1022 (m), 964 (s), 945 (s, Me_4N^+ cation), 930 (sh, Me_4N^+ cation), 855 (sh), 815 (br), 641 (s), 590 (sh) 555 (m), 465 (m), 418 (s), 343 (w) cm^{-1} . Elem anal. Calcd for $\text{C}_{12}\text{H}_{42}\text{N}_2\text{O}_{23}\text{S}_2\text{W}_5\text{Zr}_1$: C, 8.69; H, 2.54; N, 1.69. Found: C, 8.52; H, 2.62; N, 1.34.

2.a.4. Preparation of $[\text{W}_5\text{O}_{18}\text{Zr}(\text{H}_2\text{O})(\text{DMSO})_2]^{2-}$ ($\mathbf{1c}$). A suspension of complex $(\text{Me}_4\text{N})_2(\mathbf{1a})$ (0.5 g, 0.333 mmol) was refluxed in 40 mL of DMSO for 1 week. The solution was filtered to remove the excess of solute and allowed to stand at room temperature for 2 weeks, during which time small uncolored crystals were formed. A total of 0.32 g (0.188 mmol) of $(\text{Me}_4\text{N})_2(\mathbf{1c})\cdot\text{DMSO}$ was then collected (57% yield). $(\text{Me}_4\text{N})_2(\mathbf{1c})\cdot\text{DMSO}$. Raman: ν 677 (m), 715 (m), 755 (m), 834 (m), 937 (s), 965 (vs), 1010 (w) cm^{-1} . IR (KBr): ν 3036 (w), 1487 (m), 1019 (m), 962 (s), 944 (s, Me_4N^+ cation), 930 (sh, Me_4N^+ cation), 855 (sh), 813 (br), 665 (sh), 640 (s), 590 (m), 554 (m), 467 (m), 419 (s), 343 (w) cm^{-1} . ^1H NMR (CD_3SOCD_3): δ 2.54 (s, 18 H, $(\text{CH}_3)_2\text{SO}$), 3.11 (s, 24 H, $\text{N}(\text{CH}_3)_4$). ^{183}W NMR (saturated DMSO solution): δ 72.2 (s, 1 W, $J_{1/2} = 12$ Hz), 38.4 (s, 4 W, $J_{1/2} = 22$ Hz). Elem anal. Calcd for $\text{C}_{14}\text{H}_{44}\text{N}_2\text{O}_{22}\text{S}_3\text{W}_5\text{Zr}_1$: C, 9.89; H, 2.59; N, 1.65; S, 5.65; W, 54.12; Zr, 5.37. Found: C, 10.24; H, 2.74; N, 1.57; S, 5.90; W, 52.1; Zr, 5.34.

2.a.5. Preparation of $[\{\text{W}_5\text{O}_{18}\text{Zr}(\mu\text{-OH})\}_2]^{6-}$ ($\mathbf{2}$). The dimeric anion $\mathbf{2}$ was prepared according to a procedure described earlier.⁶ A total of 1.53 mL of a 1.5 M aqueous solution of $^n\text{Bu}_4\text{NOH}$ (2.30 mmol) was added to a suspension of 1.82 g (1.21 mmol) of $(\text{Me}_4\text{N})_2(\mathbf{1a})$ in 50 mL of distilled water (pH = 4). The suspension was stirred at room temperature until dissolution of the solid. After separation of a very fine insoluble powder, the resulting solution was allowed to slowly evaporate at 70 °C for 3 days. During this period, large colorless crystals of $(^n\text{Bu}_4\text{N})_6(\mathbf{2})\cdot 2\text{H}_2\text{O}$, suitable for X-ray diffraction (XRD) analysis, were formed. They were collected and dried with dimethyl ether. A total of 1 g of $^n\text{Bu}_4\text{NBr}$ was added to the liquor solution, resulting in further precipitation of $(^n\text{Bu}_4\text{N})_6(\mathbf{2})\cdot 2\text{H}_2\text{O}$ (total yield: 0.89 g, 36%) after stirring for 1 day. $(^n\text{Bu}_4\text{N})_6(\mathbf{2})\cdot 2\text{H}_2\text{O}$. Raman: ν 837 (m), 882 (w), 910 (m), 948 (s), 972 (vs) cm^{-1} . IR (KBr): ν 3680 (m), 970 (w), 945 (s), 880 (m), 810 (br), 730 (s), 640 (m), 555 (m), 435 (s), 420 (sh) cm^{-1} . ^{183}W NMR (12.5 MHz, CD_3CN , 24 °C): δ 73.6 (s, 1 W, $^2J_{\text{W-W}} = 6.2$ Hz), 47.9 (s, 4 W, $^2J_{\text{W-W}} = 6.2$ Hz). Elem anal. Calcd for $\text{C}_96\text{H}_{222}\text{N}_6\text{O}_{40}\text{W}_{10}\text{Zr}_2$: C, 27.97; H, 5.39; N, 2.04; W, 44.64; Zr, 4.43. Found: C, 27.93; H, 5.40; N, 2.04; W, 42.56; Zr, 4.18.

2.b. Crystal Structure Analysis. Single-crystal data for the Me_4N^+ salts of anions $\mathbf{1b}$ and $\mathbf{1c}$ were recorded at room temperature on a Kappa-CCD Bruker diffractometer with graphite monochromated Mo $\text{K}\alpha$ radiation ($\lambda = 0.71073$ Å) using the ω -scan technique. An orientation matrix and lattice parameters were obtained by least-squares refinement of the diffraction data of 291 reflections within the range of $4^\circ < \theta < 22^\circ$. The index ranges of data collection were $-20 \leq h \leq 20$, $-15 \leq k \leq 14$, and $-24 \leq l \leq 30$ for $(\text{Me}_4\text{N})_2(\mathbf{1b})\cdot\text{DMSO}\cdot\text{H}_2\text{O}$ and $-15 \leq h \leq 14$, $-30 \leq k \leq 27$, and $-17 \leq l \leq 21$ for $(\text{Me}_4\text{N})_2(\mathbf{1c})\cdot\text{DMSO}$. Intensity data were collected in the θ range of 2–30°; 6065 reflections for the former and 5508 for the later had $(F_o)^2 \geq 3\sigma(F_o)^2$. All of the measured independent reflections were used in the analysis. The structure was solved by direct methods and refined with a full-matrix least-squares technique on F using the *SHELXS-97*²⁰ and *CRYSTALS*²¹ programs. All non-hydrogen atoms were refined

anisotropically, except for the Me_4N^+ cations and any solvent molecules. Hydrogen atoms were not considered for refinement purposes. The values of the discrepancy indices R (wR_2) for all data were 0.0274 (0.0285) [$(\text{Me}_4\text{N})_2(\mathbf{1b})\cdot\text{DMSO}\cdot\text{H}_2\text{O}$] and 0.0368 (0.0402) [$(\text{Me}_4\text{N})_2(\mathbf{1c})\cdot\text{DMSO}$]. The final Fourier-difference map showed maximum (minimum) peak heights of 1.99 (−1.38) $\text{e}\text{Å}^{-3}$ for the former and 2.75 (−1.40) $\text{e}\text{Å}^{-3}$ for the latter, respectively. The numbers of variable parameters are 406 for $(\text{Me}_4\text{N})_2(\mathbf{1b})\cdot\text{DMSO}\cdot\text{H}_2\text{O}$ and 434 for $(\text{Me}_4\text{N})_2(\mathbf{1c})\cdot\text{DMSO}$, and the goodness-of-fits are 1.066 and 1.125, respectively. Molecular structures were drawn with the program *CAMERON*.²² CCDC 269506 [for $(\text{Me}_4\text{N})_2(\mathbf{1b})\cdot\text{DMSO}\cdot\text{H}_2\text{O}$], CCDC 272965 [for $(\text{Me}_4\text{N})_2(\mathbf{1c})\cdot\text{DMSO}$], and CCDC 229907 [for $(^n\text{Bu}_4\text{N})_6(\mathbf{2})\cdot 2\text{H}_2\text{O}$] are given in the Supporting Information and can also be obtained free of charge via www.ccdc.cam.ac.uk/conts/retrieving.html (or from the Cambridge Crystallographic Data Centre, 12 Union Road, Cambridge CB2 1EZ, U.K.; fax (+44)1223-336-033; e-mail deposit@ccdc.cam.ac.uk).

2.c. Experimental Conditions for Characterization Studies.

2.c.1. TGA–DTA. TGA–DTA measurements were performed on a TA Instruments 2960 SDT thermal analyzer. About 38 mg of $(\text{Me}_4\text{N})_2(\mathbf{1a})$ was placed inside an alumina crucible and heated at 0.167 K s^{-1} under 1.33 $\text{cm}^3 \text{s}^{-1}$ of dry N_2 up to 1073 K. An empty alumina crucible was used as the reference.

2.c.2. IR and Raman Spectroscopies. IR spectra were recorded on KBr pellets at room temperature with a Bio-Rad Win-IR FTS 165 FTIR spectrometer. Raman spectra were collected at room temperature with a Kaiser Optical Systems HL5R Raman spectrometer equipped with a near-IR laser diode working at 785 nm. The laser power was adjusted to 10–15 mW at the sample position for all spectra, and the resolution was 3 cm^{-1} .

2.c.3. Electron Paramagnetic Resonance (EPR) Spectroscopy. A few milligrams of $(\text{Me}_4\text{N})_2(\mathbf{1a})$ was placed inside an EPR tube under dynamic vacuum down to 10^{-2} Pa at room temperature. Static reduction was conducted at 573 K for 1 h in 200 Torr of hydrogen followed by sample evacuation to 10^{-2} Pa. EPR spectra were recorded at 77 K in a vacuum on a Bruker ESP 300E spectrometer operated at 9.3 GHz (X band) with a 100-kHz field modulation and a 10-G modulation amplitude. The microwave power and frequency were 10 mW and 9.25 GHz, respectively. EPR spectra were collected both before and after the reduction treatment. EPR simulations were carried out using a DOS-modified version of SIM14S software.²³

2.c.4. Zr K-Edge Extended X-ray Absorption Fine Structure (EXAFS). X-ray absorption spectroscopy data were collected at the Elettra synchrotron light source (Italy) using channel-cut silicon (111) crystals. The electron energy and the ring current were 2.4 GeV and 150 mA, respectively. The Zr K-edge spectrum of compound $(\text{Me}_4\text{N})_2(\mathbf{1a})$ was recorded in the transmission mode in air at 77 K using ion chambers. The sample was thoroughly ground, mixed with cellulose, and pelletized in order to yield an absorption coefficient μ of 2–3. Calibration of the monochromator was performed with a Zn metal foil. The energy was scanned with incremental energy steps of 3 eV/2 s from 17 800 to 19 000 eV. Up to four scans were collected for each sample for a total analysis time of about 1 h. Raw data were interpolated to 2-eV steps and averaged into a single absorption coefficient $\mu(E)$ for each sample.

(21) Watkin, D. J.; Carruthers, J. R.; Betteridge, P. W. *CRYSTALS*; Chemical Crystallography Laboratory, University of Oxford: Oxford, U.K., 1996.

(22) Pearce, L. J.; Watkin, D. J. *CAMERON*; Chemical Crystallography Laboratory, University of Oxford: Oxford, U.K., 1996.

(23) Lozos, G. P.; Hoffman, B. M.; Franz, C. G. *QCPE* **1974**, *11*, 265.

(20) Sheldrick, G. M. *SHELXS-97*; University of Göttingen: Göttingen, Germany, 1997.

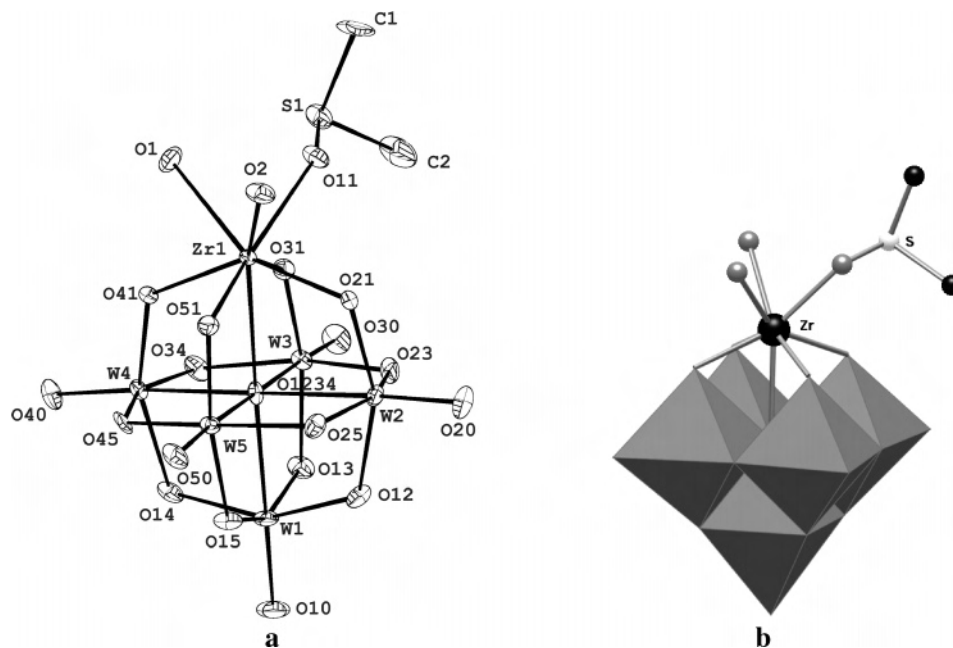


Figure 1. Ball-and-stick (a) and polyhedral (b) representations of the anion **1b**: $[\text{W}_5\text{O}_{18}\text{Zr}(\text{H}_2\text{O})_2(\text{DMSO})]^{2-}$.

EXAFS data extraction and simulation were performed by standard procedures using Michalowicz's software package.²⁴ Fourier transforms (FT) of $w(k) k^2\chi(k)$ EXAFS data [$w(k)$ is a Kaiser–Bessel window with a smoothness parameter of 3.0] were then carried out in the range of $\Delta k = 3.0\text{--}15.8 \text{ \AA}^{-1}$ in order to obtain a radial distribution function (RDF). The FT was filtered in the 1.2–4.0- \AA range for compound $(\text{Me}_4\text{N})_2(\mathbf{1a})$ and in the 0.9–4.0- \AA range for compound $(^n\text{Bu}_4\text{N})_6(\mathbf{2})\cdot 2\text{H}_2\text{O}$ and then back-Fourier-transformed to be fitted in the k space. Multiple shell fitting was carried out using the EXAFS plane wave approximation and excluding any multiple scattering paths. The quality of the fit was estimated according to the agreement factor (ρ) defined in eq 1.

$$\rho (\%) = 100 \times \frac{\sum (k\chi_{\text{exp}} - k\chi_{\text{th}})^2}{\sum (k\chi_{\text{exp}})^2} \quad (1)$$

Phase shifts and amplitudes for the single atomic pairs Zr–O (at 1.90 \AA), Zr–W (at 3.30 \AA), and Zr–Zr (3.63 \AA) were theoretically derived from first principles using the FEFF8.20 code.²⁵

3. Results and Discussion

3.a. Syntheses. The synthesis of $(\text{Me}_4\text{N})_2(\mathbf{1a})$ results from the slow self-condensation of simple $[\text{WO}_4]^{2-}$ anions with Zr^{IV} cations in an aqueous acidic medium (cf. section 2.a). The compound crystallizes as a pure Me_4N^+ salt but could not be directly isolated from alkaline cations such as Cs^+ . $(\text{Me}_4\text{N})_2(\mathbf{1a})$ was used as a precursor for the synthesis of the dimeric anion $(^n\text{Bu}_4\text{N})_6(\mathbf{2})\cdot 2\text{H}_2\text{O}$ by alkalization with $^n\text{Bu}_4\text{NOH}$ of a diluted aqueous solution of $(\text{Me}_4\text{N})_2(\mathbf{1a})$.⁶ We did not succeed in obtaining suitable crystals of $(\text{Me}_4\text{N})_2(\mathbf{1a})$ for X-ray study by recrystallization in most common solvents or mixtures thereof. However, slow recrystallization of $(\text{Me}_4\text{N})_2(\mathbf{1a})$ in hot DMSO allowed us to obtain small crystals

of $(\text{Me}_4\text{N})_2(\mathbf{1b})\cdot \text{DMSO}\cdot \text{H}_2\text{O}$ (Figure 1) or $(\text{Me}_4\text{N})_2(\mathbf{1c})\cdot \text{DMSO}$ (Figure 2), depending on the experimental conditions. Refluxing the suspension of $(\text{Me}_4\text{N})_2(\mathbf{1a})$ in a 1:1 mixture of water/DMSO for 1 h, followed by filtration of the solute excess, leads to a very slow replacement of a water molecule in $(\text{Me}_4\text{N})_2(\mathbf{1a})$ by a DMSO molecule. It is noteworthy that crystals of $(\text{Me}_4\text{N})_2(\mathbf{1b})\cdot \text{DMSO}\cdot \text{H}_2\text{O}$ were obtained after allowing the solution to stand at room temperature for 2 months. It seems that this period cannot be shortened because the untimely addition of diethyl ether led to the precipitation of the starting anion $(\text{Me}_4\text{N})_2(\mathbf{1a})$. The replacement of a second water molecule by a supplementary DMSO molecule occurred by prolonging the reflux period of the initial suspension of $(\text{Me}_4\text{N})_2(\mathbf{1a})$ by 1 week. Crystals of $(\text{Me}_4\text{N})_2(\mathbf{1c})\cdot \text{DMSO}$ were formed at room temperature after filtration of the insoluble powder.

3.b. Crystal Structures of Anions **1b and **1c**.** The structures of the bivalent anions **1b** and **1c** (Table 1) are shown in Figures 1 and 2, respectively. They are closely related to that of the so-called Lindqvist structure with the general formula $[\text{M}_6\text{O}_{19}]^{n-}$ ($\text{M} = \text{Mo}^{\text{VI}}, \text{W}^{\text{VI}}, \text{V}^{\text{V}},$ and Nb^{V}). They derive from the octahedral structure of $[\text{W}_6\text{O}_{19}]^{2-}$ by the replacement of one $\{\text{WO}\}^{4+}$ group by a $\{\text{Zr}(\text{H}_2\text{O})_{3-n}(\text{DMSO})_n\}^{4+}$ isocharged group. In this compound, Zr adopts an 8-fold coordination because it is bound to five O atoms from the $\{\text{W}_5\text{O}_{18}\}^{6-}$ subunits and three O atoms from the solvent molecules (one DMSO and two water molecules for anion **1b** and two DMSO units and one water molecule for anion **1c**). Because of the hardness of the Zr^{IV} cation, the DMSO ligand is preferentially bound through the O atom rather than the S atom. The Zr–O distances in **1b** and **1c** are comparable (Table 2). They are in the range of 2.073 (Zr1–O31, **1c**) to 2.603 \AA (Zr1–O1234, i.e., the central $\{\mu^6\text{-O}\}^{2-}$ anion, **1c**).

For the sake of clarity, the structures of **1b** and **1c** may be compared to that of the dimeric anion **2**, in which the

(24) Michalowicz, A. *Logiciels pour la Chimie*; Société Française de Chimie: Paris, 1991; p 102.

(25) Ankudinov, A. L.; Ravel, B.; Rehr, J. J.; Conradson, S. D. *Phys. Rev. B* **1998**, *58*, 7565.

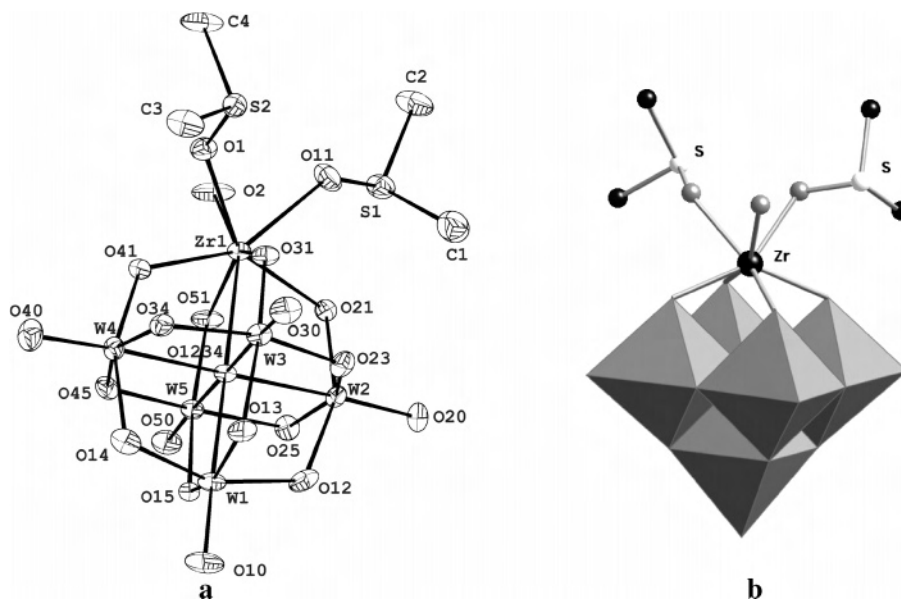


Figure 2. Ball-and-stick (a) and polyhedral (b) representations of the anion **1c**: $[\text{W}_5\text{O}_{18}\text{Zr}(\text{H}_2\text{O})(\text{DMSO})_2]^{2-}$.

Table 1. Crystal Data for Compounds $(\text{Me}_4\text{N})_2(\mathbf{1b})\cdot\text{DMSO}\cdot\text{H}_2\text{O}$ and $(\text{Me}_4\text{N})_2(\mathbf{1c})\cdot\text{DMSO}$

	$(\text{Me}_4\text{N})_2(\mathbf{1b})\cdot\text{DMSO}\cdot\text{H}_2\text{O}$	$(\text{Me}_4\text{N})_2(\mathbf{1c})\cdot\text{DMSO}$
formula	$\text{C}_{12}\text{H}_{42}\text{N}_2\text{O}_{23}\text{S}_2\text{W}_5\text{Zr}_1$	$\text{C}_{14}\text{H}_{44}\text{N}_2\text{O}_{22}\text{S}_3\text{W}_5\text{Zr}_1$
M_r [g mol^{-1}]	1657.07	1699.17
color	colorless	colorless
cryst syst	monoclinic	monoclinic
space group	$P2_1/c$	$P2_1/n$
T (K)	ambient	ambient
a [Å]	14.8962(14)	11.0093(7)
b [Å]	10.8357(6)	21.9461(19)
c [Å]	21.9071(17)	15.1748(18)
α [deg]	90	90
β [deg]	101.337(6)	91.245(8)
γ [deg]	90	90
V [Å ³]	3467.1(4)	3665.5(5)
Z	4	4
μ [cm^{-1}]	17.016	16.151
ρ_{calcd} [g cm^{-3}]	3.17	3.08
$\theta_{\text{min}}-\theta_{\text{max}}$ [deg]	2–30	2–30
octants collected	–20, 20; –15, 14; –24, 30	–15, 14; –30, 27; –17, 21
measd reflns	22 279	26 745
unique reflns (R_{int})	9746 (0.030)	10645 (0.044)
obsd reflns	$6065(F_o)^2 > 3\sigma(F_o)^2$	$5508(F_o)^2 > 3\sigma(F_o)^2$
abs correction	sadabs	sadabs
refined param	406	434
R	0.0274	0.0368
R_w	0.0285 ^a	0.0402
goodness of fit S	1.0657	1.0912
$\Delta\rho$ (max/min) [e Å^{-3}]	1.99/–1.38	2.75/–1.40

^a Weighting scheme of the form $w = w' \{1 - [(|F_o| - |F_c|)/6\sigma(F_o)]^2\}$ with $w' = 1/\sum_i A_i T_i(X)$ with coefficients 0.956, –0.281, 0.724, –0.0612, and 0.127 for $(\text{Me}_4\text{N})_2(\mathbf{1b})\cdot\text{DMSO}\cdot\text{H}_2\text{O}$ and 2.07, –0.716, and 1.57 for $(\text{Me}_4\text{N})_2(\mathbf{1c})\cdot\text{DMSO}$ for a Chebyshev series for which $X = F_c/F_o(\text{max})$.

Zr^{IV} cation is seven-coordinated to five O atoms of the $\{\text{W}_5\text{O}_{18}\}^{6-}$ core and to two $\mu\text{-OH}^-$ ligands (Figure 3). The Zr^{IV} cation, because of its large ionic radius, commonly attains high coordination numbers, for example, 7 (for anion **2**) and 8 (for anions **1b** and **1c**). In the case of eight-coordinated complexes, the geometry could be either square-antiprism $\text{Zr}(\text{acac})_4$ ²⁶ or $\text{Zr}(\text{SO}_4)_2\cdot 4\text{H}_2\text{O}$ ²⁷ or dodecahedral

Table 2. Selected Bond Distances in Anions **1b**, **1c**, and **2**

	1b	1c	2		
Zr1–O1	2.277(6)	Zr1–O1	2.243(8)	Zr1–O11	2.135(9)
Zr1–O2	2.324(5)	Zr1–O2	2.259(9)	Zr1–O11'	2.177(8)
Zr1–O11	2.244(5)	Zr1–O11	2.291(9)	Zr1–O21	2.107(9)
Zr1–O21	2.080(5)	Zr1–O21	2.100(8)	Zr1–O31	2.09(1)
Zr1–O31	2.093(5)	Zr1–O31	2.073(8)	Zr1–O41	2.058(9)
Zr1–O41	2.138(5)	Zr1–O41	2.105(8)	Zr1–O51	2.109(9)
Zr1–O51	2.119(5)	Zr1–O51	2.124(8)	Zr1–O2345	2.371(8)
Zr1–O1234	2.562(5)	Zr1–O1234	2.603(8)		

$[\text{Zr}(\text{C}_2\text{O}_4)_4]^{4-}$ ²⁸ The local geometry around the Zr^{IV} cation in anions **1b** and **1c** can be described as a distorted dodecahedron with a particularly long distance (2.6 Å) to one of the ligands. The geometrical characteristics of the $\{\text{W}_5\text{O}_{18}\}^{6-}$ core remain essentially similar to those of other substituted Lindqvist-type complexes²⁹ and especially to the dimeric $[\{\text{W}_5\text{O}_{18}\text{Zr}(\mu\text{-OH})_2\}]^{6-}$ anion **2**. All of these complexes, together with their geometries, thus provide different models for Zr K-edge EXAFS spectroscopy, in terms of the coordination number and nature of the ligands.

3.c. IR and Raman Results. The IR bands of compounds $(\text{Me}_4\text{N})_2(\mathbf{1a})$, $(\text{Me}_4\text{N})_2(\mathbf{1b})\cdot\text{DMSO}\cdot\text{H}_2\text{O}$, $(\text{Me}_4\text{N})_2(\mathbf{1c})\cdot\text{DMSO}$, and $(\text{Bu}_4\text{N})_6(\mathbf{2})\cdot 2\text{H}_2\text{O}$ are reported in section 2.a and exhibit characteristic features of substituted Lindqvist-type polyoxoanions. Indeed, it is well-known that the IR spectrum of the hexatungstate $[\text{W}_6\text{O}_{19}]^{2-}$ anion (which displays O_h symmetry) shows a strong and highly symmetric $\nu_s(\text{W}=\text{O}_i)$ stretching band at 996 cm^{-1} .⁶ Splitting of the $\nu_s(\text{W}=\text{O}_i)$ band is expected to occur in substituted anions **1a**, **1b**, and **1c** because of the loss of symmetry. However, the presence of a sharp band due to the Me_4N^+ counterion in this region (945 cm^{-1}) complicates the analysis. Furthermore, as has

(27) Singer, J.; Cromer, D. T. *Acta Crystallogr.* **1959**, *12*, 719.

(28) Allard, B. *J. Inorg. Nucl. Chem.* **1976**, *38*, 2109.

(29) Iball, J.; Low, J. N.; Weakley, T. J. R. *J. Chem. Soc., Dalton Trans.* **1974**, 2021. Angus-Dunne, S. J.; Burns, R. C.; Craig, D. C.; Lawrence, G. A. *J. Chem. Soc., Chem. Commun.* **1994**, 523. Yamase, T.; Ozeki, T.; Tosaka, M. *Acta Crystallogr., C* **1994**, *50*, 1849. Artero, V.; Proust, A.; Herson, P.; Gouzerh, P. *Chem.—Eur. J.* **2001**, *7*, 3901.

(26) Silvertown, J. V.; Hoard, J. F. *Inorg. Chem.* **1963**, *2*, 243.

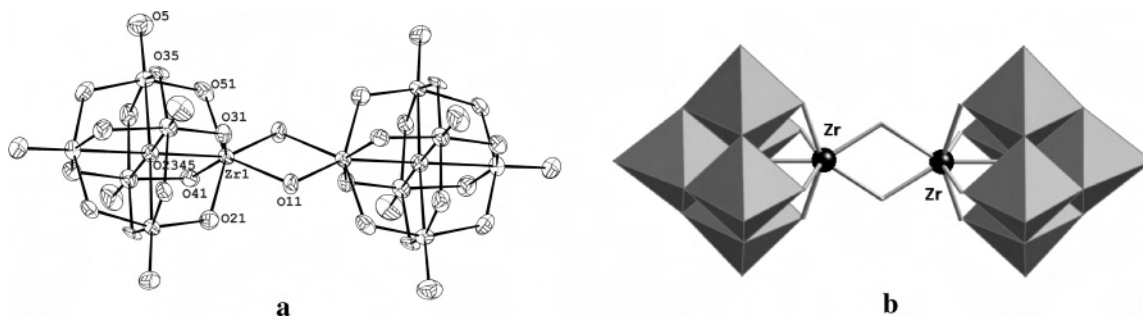


Figure 3. Ball-and-stick (a) and polyhedral (b) representations of the anion **2**: $[\{W_5O_{18}Zr(\mu-OH)\}_2]^{6-}$.

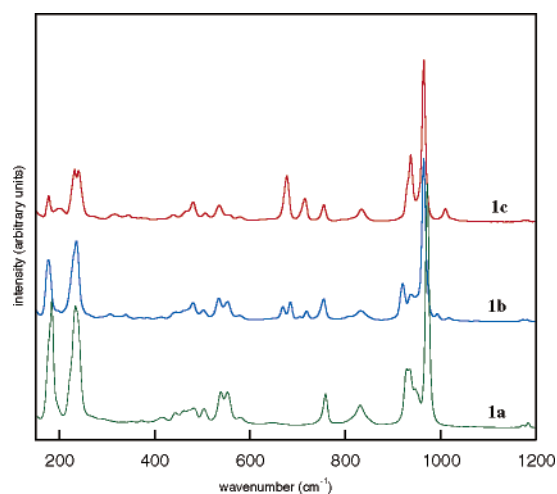


Figure 4. Raman spectra of $(Me_4N)_2(\mathbf{1a})$, $(Me_4N)_2(\mathbf{1b})\cdot DMSO\cdot H_2O$, and $(Me_4N)_2(\mathbf{1c})\cdot DMSO$.

been previously observed for other substituted hexatungstates, the replacement of a W atom by a Zr atom in the structure is expected to lead to the global decrease of the energy of the $\nu(M-O)$ bands³⁰ that reflects on the corresponding force constants. Therefore, the $\nu_s(W=O_t)$ vibrational frequency is shifted to 972 cm^{-1} for compounds $(Me_4N)_2(\mathbf{1a})$ and $(^nBu_4N)_6(\mathbf{2})\cdot 2H_2O$ and to 965 cm^{-1} for the DMSO-containing compounds $(Me_4N)_2(\mathbf{1b})\cdot DMSO\cdot H_2O$ and $(Me_4N)_2(\mathbf{1c})\cdot DMSO$.

As shown in Figure 4, the Raman spectra of compounds $(Me_4N)_2(\mathbf{1a})$, $(Me_4N)_2(\mathbf{1b})\cdot DMSO\cdot H_2O$, and $(Me_4N)_2(\mathbf{1c})\cdot DMSO$ are quite similar and contain vibrational features of monosubstituted Lindqvist-type polyoxoanions, which have been discussed elsewhere.^{30,31} It is noteworthy that the spectra of $(Me_4N)_2(\mathbf{1b})\cdot DMSO\cdot H_2O$ and $(Me_4N)_2(\mathbf{1c})\cdot DMSO$ show additional bands ascribed to DMSO molecules (which are present as either ligands or crystallization molecules) in the range of $650\text{--}750\text{ cm}^{-1}$ and beyond 1000 cm^{-1} .

The high-frequency Raman band at 972 cm^{-1} in $(Me_4N)_2(\mathbf{1a})$ and 996 cm^{-1} in $(^nBu_4N)_2[W_6O_{19}]$ is ascribed to the symmetric stretching mode (A_{1g}) of the $W=O_t$ terminal groups.⁶ The corresponding antisymmetric stretching mode (E_u) is also shifted from 971 to 928 cm^{-1} upon Zr insertion into the hexatungstic core. Replacing W with Zr is also at the origin of the $840\text{--}831\text{ cm}^{-1}$ band shift of the antisym-

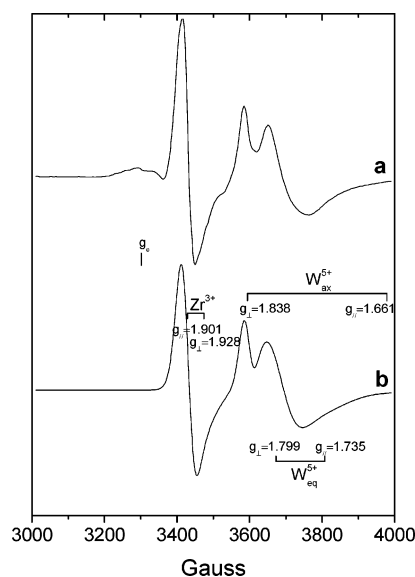


Figure 5. Experimental (a) and simulated (b) EPR spectra (X band, 77 K) of $(Me_4N)_2(\mathbf{1a})$ partially reduced for 1 h at 573 K in 200 Torr of static H_2 . The axial paramagnetic features ascribed to Zr^{3+} , W_{ax}^{5+} , and W_{eq}^{5+} species (Table 3) are shown.

metric mode of bridging $W-O_b$ bonds, while a symmetry loss leads to splitting of the corresponding symmetric mode in the $400\text{--}600\text{ cm}^{-1}$ range. Low-frequency bands ($150\text{--}300\text{ cm}^{-1}$), ascribed to $W-O_b-W$ bending modes, remain practically unchanged as expected if the Lindqvist structure is preserved in anions **1a**, **1b**, and **1c**.

Taking into account the very similar IR and Raman data, it is clear that the structures of the three anions **1a**, **1b**, and **1c** are structurally very similar and that small differences arise from different chemical environments around the Zr^{IV} cation.

3.d. EPR Results on Partially Reduced $(Me_4N)_2(\mathbf{1a})$. The EPR spectrum of a solid sample of $(Me_4N)_2(\mathbf{1a})$, partially reduced in H_2 at 573 K for 1 h, is represented in Figure 5. Computer simulations were carried out by considering several models, taking into account a Lindqvist structure for **1a** closely related to that of **1b** and **1c**. As illustrated in Figure 5, the best fit is found when three axial contributions are considered. The corresponding magnetic parameters are provided in Table 3.

The most intense contribution shows a magnetic feature at $g_{\parallel} = 1.901$, with a relatively broad perpendicular feature (80 G) at $g_{\perp} = 1.928$. This resonance line could not be ascribed to W^V ions because the corresponding signals (Table

(30) Rocchiccioli-Deltcheff, C.; Thouvenot, R.; Dabbabi, M. *Spectrosc. Acta A* **1977**, *33*, 143.

(31) Rocchiccioli-Deltcheff, C.; Fournier, M.; Franck, R.; Thouvenot, R. *J. Mol. Struct.* **1984**, *114*, 49.

3) responded differently upon varying the spectrum recording temperature. Namely, the signals at $g_{\perp} = 1.928$ and $g_{\parallel} = 1.901$ were clearly visible, whereas the other magnetic features remained practically absent at 298 K. Instead, we propose to assign this signal to Zr^{III} reduced ions, in coherence with the relative populations shown in Table 3 [exptl, Zr^{III} 21%; calcd, Zr^{III} 16.7%, in $(Me_4N)_2(\mathbf{1a})$]. Torralvo et al.³² first reported an EPR axial resonance at $g_{\perp} = 1.981$ and $g_{\parallel} = 1.956$ ascribed to Zr^{3+} ions present in monoclinic ZrO_2 . The deviation from the g values reported here is likely to reflect distinct crystal-field energies because the local environment surrounding Zr^{3+} ions differs in monoclinic ZrO_2 (7-fold coordination) and in anion $\mathbf{1a}$ (8-fold coordination).

The other two axial signals with g_{\perp} components at 1.838 and 1.799 are ascribed to W^V -reduced ions, in agreement with the results of Kuba et al. after the reduction of WO_3/ZrO_2 catalysts.¹⁵ The simulation results indicate that the first type of W ($g_{\perp} = 1.838$) contributes 17% while the second type ($g_{\perp} = 1.799$) contributes 62% to the whole spectrum. These quantitative findings are in good agreement with those expected from the structure of the substituted Lindqvist anion. In this anion, with approximate C_{4v} symmetry, there are two distinct types of W sites: four W atoms in equatorial positions sharing edges with the $\{Zr(H_2O)_3\}^{4+}$ group and one W atom lying in the axial position and linked through one common apex with the $\{Zr(H_2O)_3\}^{4+}$ group. The W atoms located at these two types of sites experience different magnetic environments because of the vicinity of Zr, and this will reflect on the corresponding magnetic parameters. The quantitative data seem to suggest a statistical distribution of the unpaired electron over all metallic centers, which implies full mobility throughout the cluster, even at 77 K, probably because of an electron-hopping effect.³³ Ab initio calculations are currently in progress to shed more light on this issue.

The axial signals found on the EPR spectrum (Figure 5) are typical of octahedral crystal fields with significant tetragonal distortion. This happens because W atoms are displaced toward terminal O atoms. For W^V (d^1) ions, the following g -tensor expressions hold for a compressed octahedron (eqs 2 and 3),³⁴ where $\delta = E_{yz,zx} - E_{xy}$,

$$g_{\perp} = g_e - \frac{2\lambda}{\delta} \quad (2)$$

$$g_{\parallel} = g_e - \frac{8\lambda}{\Delta} \quad (3)$$

$\Delta = E_x^2 - y^2 - E_{xy}$, and λ is the spin-orbit coupling constant. Spin-orbit constant λ is positive for d^1 ions, and therefore g values are expected to be observed at $g < g_e$ and to depend on the energy gap between the ground and

Table 3. Magnetic Parameters Obtained by Simulation of the EPR Spectrum of $(Me_4N)_2(\mathbf{1a})$ Partially Reduced in Hydrogen^a

paramagnetic center	g_{\perp}	g_{\parallel}	ΔH_{\perp} (G)	ΔH_{\parallel} (G)	contribution to the total spectrum (%)	tetragonal distortion (δ/Δ)
Zr^{III}	1.928	1.901	80	36	21	na
W^V ax	1.838	1.661	29	131	17	0.52
W^V eq	1.799	1.735	88	150	62	0.33

^a The signal width is denoted by ΔH . The relative tetragonal distortion is presented as crystal-field energies ratio δ/Δ . $\delta = (E_{yz,zx} - E_{xy})$, and $\Delta = (E_x^2 - y^2 - E_{xy})$.

excited states. Tetragonal distortion changes the crystal-field energy and leads to a decrease in Δ and an increase in δ . Equations 2 and 3 may be combined in the form of eq 4, which allows one to estimate the relative extent of tetragonal distortion δ/Δ inside an octahedral crystal field.³⁵

$$\frac{\delta}{\Delta} = \frac{1}{4} \frac{g_e - g_{\parallel}}{g_e - g_{\perp}} \quad (4)$$

The magnetic parameters in Table 3 were used to compute the relative distortion degree for both types of W^V -reduced ions in $(Me_4N)_2(\mathbf{1a})$. The data show that W atoms in the equatorial positions (i.e., vicinal to the Zr atom) are less distorted compared to the W atom in the axial position. Accordingly, the crystal structure of compound $(Me_4N)_2(\mathbf{1b}) \cdot DMSO \cdot H_2O$, for instance, reveals a longer distance between the axial W and the central O_c atom (2.368 Å) when compared to the average $W-O_c$ distance of the equatorial $\{WO_6\}^{6-}$ octahedra (2.317 Å).

3.e. Zr K-Edge EXAFS Results on Compound $(Me_4N)_2(\mathbf{1a})$. EXAFS data are particularly helpful in the case of $(Me_4N)_2(\mathbf{1a})$ because no X-ray crystal structure of this compound is available. However, it is possible to gain insight into the local structure around Zr in the structure of $(Me_4N)_2(\mathbf{1a})$ by comparison of EXAFS data with the crystal structure of compound $(Me_4N)_2(\mathbf{1b}) \cdot DMSO \cdot H_2O$ because both compounds are believed to be structurally similar according to IR and Raman data.

The RDF of compound $(Me_4N)_2(\mathbf{1a})$ is presented in Figure 6 along with the imaginary part. Two peaks can be noticed in the magnitude plot of the FT. The first peak is found at a short distance (ca. 1.5 Å) and is due to the first O shell surrounding the Zr atom. The second peak is found near 3.1 Å and is due to the four W atoms in the second coordination sphere around Zr. It has to be noted that these distances do not represent true interatomic distances because they were not corrected for phase shift.

The first coordination sphere around Zr in $(Me_4N)_2(\mathbf{1b}) \cdot DMSO \cdot H_2O$ is entirely made up of O atoms held at different distances that can be grouped into three families: four bridging O atoms (O_b) linking Zr and W whose distances vary from 2.081 to 2.139 Å; three terminal O atoms (O_t) ascribed to two water molecules and one DMSO molecule whose distances range from 2.245 to 2.324 Å, and one O atom (O_c) placed in the center of the Lindqvist structure at 2.562 Å. A single O shell could not accurately fit the first

(32) Torralvo, M. J.; Alario, M. A.; Soria, J. *J. Catal.* **1984**, *86*, 473.

(33) Sanchez, C.; Livage, J.; Launay, J. P.; Fournier, M. *J. Am. Chem. Soc.* **1983**, *105*, 6817.

(34) Che, M.; Bozon-Verduraz, F. In *Handbook of Heterogeneous Catalysis*; Knözinger, H., Weitkamp, J., Ertl, G., Eds.; Wiley-VCH: Weinheim, Germany, 1997; Vol 3, p 641. Dyrek, K.; Che, M. *Chem. Rev.* **1997**, *97*, 305.

(35) Dufaux, M.; Che, M.; Naccache, C. *J. Chim. Phys.* **1970**, *67*, 527.

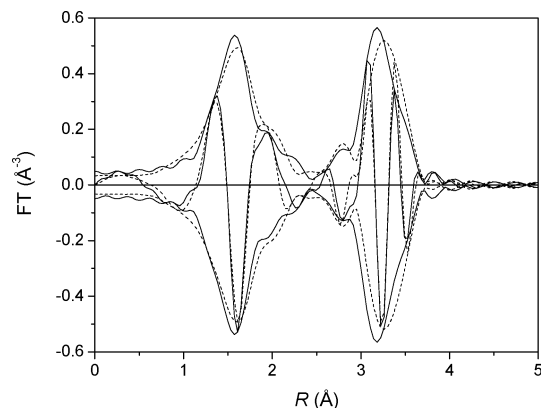


Figure 6. FT modulus and imaginary part of the EXAFS signal (k^2 -weighted) at the Zr K edge of $(\text{Me}_4\text{N})_2(\mathbf{1a})$: experimental (full line) and simulated (dotted line) spectra.

Table 4. Structural Parameters Derived from Fitting of the EXAFS Spectra Shown in Figures 6 and 7 at the Zr K Edge

compound	back-scatterer	N^a	R (Å) ^a	σ (Å)	ΔE_0 (eV)	ρ (%)
$(\text{Me}_4\text{N})_2(\mathbf{1a})$	O _b	4	2.11	0.081	3.0	4.5
	O _t	3	2.28	0.080		
	W	4	3.45	0.068	1.1	
$(^n\text{Bu}_4\text{N})_6(\mathbf{2})\cdot 2\text{H}_2\text{O}$	O _b	4	2.09	0.073	1.0	7.3
	O _{μ}	2	2.16	0.044		
	O _c	1	2.37	0.090		
	W	4	3.36	0.058	-6.1	
	Zr	1	3.63	0.055	-4.1	

^a Coordination numbers (N) and distances (R) were kept fixed during the fit and were equal to the average crystallographic values of $(\text{Me}_4\text{N})_2(\mathbf{1b})\cdot\text{DMSO}\cdot\text{H}_2\text{O}$ to fit $(\text{Me}_4\text{N})_2(\mathbf{1a})$ and to published data⁶ to fit $(^n\text{Bu}_4\text{N})_6(\mathbf{2})\cdot 2\text{H}_2\text{O}$.

peak in the EXAFS spectrum of $(\text{Me}_4\text{N})_2(\mathbf{1a})$, and hence a two-shell model was considered that comprised the four bridging O atoms (O_b) as well as three terminal O atoms (O_t). The addition of a third shell due to the central O atom (O_c) did not improve the quality of the fit and therefore was ruled out. The coordination numbers (N) and interatomic distances (R) were kept fixed at the mean crystallographic values of $(\text{Me}_4\text{N})_2(\mathbf{1b})\cdot\text{DMSO}\cdot\text{H}_2\text{O}$, and only the Debye–Waller factors (σ) and ΔE_0 were allowed to vary (Table 4). Multiple scattering effects were found to be negligible by computing the theoretical EXAFS spectra with and without taking it into account.

As shown in Figure 6, a good fit is obtained with two O shells. In the second coordination sphere around Zr, the main contribution comes from the W atoms. According to the crystallographic distances for compound $(\text{Me}_4\text{N})_2(\mathbf{1b})\cdot\text{DMSO}\cdot\text{H}_2\text{O}$, four W backscatterers are expected in the range of 3.432–3.467 Å, which correspond to the four $\{\text{WO}_6\}^{6-}$ groups in the equatorial position of the Lindqvist structure. Accordingly, the second peak in the RDF of $(\text{Me}_4\text{N})_2(\mathbf{1a})$ is well described by considering four W atoms at an average distance of 3.45 Å (Table 4).

A good agreement between experimental and simulated spectra is obtained with only three shells, taking into account the crystallographic parameters of $(\text{Me}_4\text{N})_2(\mathbf{1b})\cdot\text{DMSO}\cdot\text{H}_2\text{O}$ (Figure 6). A slight misfit occurs in the W shell probably because of the missing contribution due to the four O atoms that bind the equatorial $\{\text{WO}_6\}^{6-}$ groups together. These

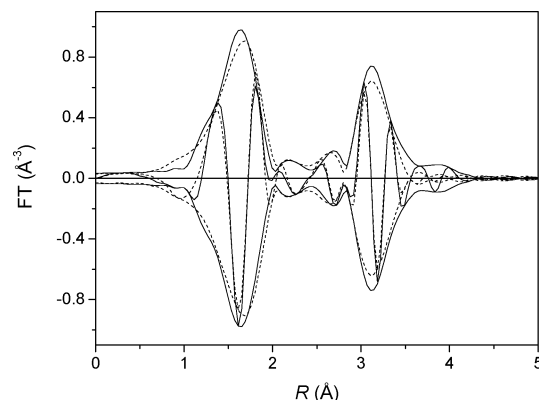


Figure 7. FT modulus and imaginary part of the EXAFS signal (k^2 -weighted) at the Zr K edge of $(^n\text{Bu}_4\text{N})_6(\mathbf{2})\cdot 2\text{H}_2\text{O}$: experimental (full line) and simulated (dotted line) spectra.

bridging O atoms can be found at distances ranging from 3.697 to 3.792 Å in $(\text{Me}_4\text{N})_2(\mathbf{1b})\cdot\text{DMSO}\cdot\text{H}_2\text{O}$ but have a limited contribution to the second peak, especially at high k weightings, as a consequence of the amplitude dependence on energy.

Because the EXAFS spectrum of $(\text{Me}_4\text{N})_2(\mathbf{1a})$ could be well depicted on the basis of crystallographic data of compound $(\text{Me}_4\text{N})_2(\mathbf{1b})\cdot\text{DMSO}\cdot\text{H}_2\text{O}$, the zirconium-substituted anions $[\text{W}_5\text{O}_{18}\text{Zr}(\text{H}_2\text{O})_{3-n}(\text{DMSO})_n]^{2-}$ ($n = 0, 1,$ and 2) can be considered as structurally identical.

For the sake of comparison, the Zr K-edge EXAFS spectrum of compound $(^n\text{Bu}_4\text{N})_6(\mathbf{2})\cdot 2\text{H}_2\text{O}$, where the Zr atom is seven-coordinated, is also included in the discussion (Figure 7). Similarly, the backscatterer contributions were grouped as previously, and the coordination numbers as well as interatomic distances were kept fixed at their mean crystallographic values,⁶ while the disorder terms (σ) and energy shift corrections (ΔE_0) were refined in order to fit the experimental spectrum. The simulation results are shown in Table 4. Four bridging oxygens (O_b) were taken at 2.09 Å, as well as two oxygen atoms at 2.16 Å from the bridging OH groups that link the two oxotungstic caps (Figure 3). However, in contrast to the situation prevailing for $(\text{Me}_4\text{N})_2(\mathbf{1a})$, the contribution due to the central O atom O_c was found to be important in $(^n\text{Bu}_4\text{N})_6(\mathbf{2})\cdot 2\text{H}_2\text{O}$ to correctly depict the first peak, although its disorder term is somewhat high (0.090 Å). This may be related to the shorter Zr–O_c distance in $(^n\text{Bu}_4\text{N})_6(\mathbf{2})\cdot 2\text{H}_2\text{O}$ (2.37 Å) compared to that in $(\text{Me}_4\text{N})_2(\mathbf{1a})$ [estimated value 2.56 Å according to $(\text{Me}_4\text{N})_2(\mathbf{1b})\cdot\text{DMSO}\cdot\text{H}_2\text{O}$] and consequently higher backscattering amplitude. Regarding the second coordination sphere, the four W atoms are found at 3.36 Å, i.e., closer to Zr than in $(\text{Me}_4\text{N})_2(\mathbf{1a})$. Additionally, one contribution due to the Zr–Zr pair at 3.63 Å had to be considered to improve the quality of the fit around the second peak. This contribution arises from the Zr atoms involved in the bridge linking the two $\{\text{W}_5\text{O}_{18}\text{Zr}(\text{OH})\}^{3-}$ units.

3.f. TGA–DTA of $(\text{Me}_4\text{N})_2(\mathbf{1a})$. Crystallographic resolution of compound $(\text{Me}_4\text{N})_2(\mathbf{1a})$ was impossible, and hence determination of the number of water molecules was achieved by means of TGA. The thermogram shown in Figure 8 shows two major weight losses both associated with

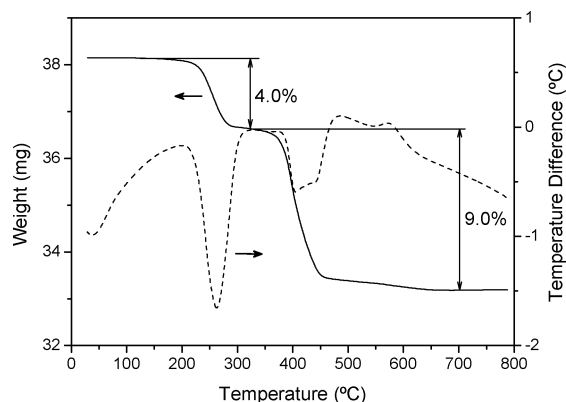


Figure 8. TGA–DTA of $(\text{Me}_4\text{N})_2(\mathbf{1a})$ under a N_2 atmosphere: TGA (full line) and DTA (dashed line) curves.

endothermic events. The first peak occurs at fairly high temperature ($263\text{ }^\circ\text{C}$) and agrees with the loss of three water molecules covalently bound to Zr (exptl, 4.0%; calcd, 3.6%). The second peak found near $400\text{ }^\circ\text{C}$ arises from the destruction of the organic cation Me_4N^+ (exptl, 9.0%; calcd, 9.9%). Hence, TGA provides further evidence that Zr atoms in anion **1a** adopt an 8-fold coordination, like in anions **1b** and **1c**, in good agreement with EXAFS and Raman results.

3.g. Relevance to the Study of Tungstated Zirconia Catalysts. It is instructive to look more closely at the surface structures of WZ catalysts. An EXAFS study revealed the presence of Zr^{IV} ions in the second coordination sphere around W atoms of the supported WO_x phase.³⁶ This finding supports the proposal of Scheithauer et al.,¹⁴ who claimed the formation of a pseudo-heteropolyacid overlayer to be responsible for the acidity of WZ catalysts. Moreover, it is well-known that an active WZ catalyst requires the formation of a metastable tetragonal zirconia phase, while monoclinic zirconia yields essentially inactive solids.¹² It is known that Zr^{IV} adopts an 8-fold coordination in tetragonal zirconia and is seven-coordinated in the monoclinic polymorph.³⁷ Interestingly, in compounds $(\text{Me}_4\text{N})_2(\mathbf{1a})$, $(\text{Me}_4\text{N})_2(\mathbf{1b})\cdot\text{DMSO}\cdot\text{H}_2\text{O}$, and $(\text{Me}_4\text{N})_2(\mathbf{1c})\cdot\text{DMSO}$ described in this work, the Zr^{IV} atoms also adopt an 8-fold coordination. Moreover, the average number of W neighbors surrounding each W atom in these zirconium isopolytungstates (ca. four) lies within the range found over the most active samples of WZ (ca. three to four).³⁸

(36) Wong, S.-T.; Li, T.; Cheng, S.; Lee, J.-F.; Mou, C.-Y. *J. Catal.* **2003**, *215*, 45.

(37) Howard, C. J.; Hill, R. J.; Reichert, B. E. *Acta Crystallogr., B* **1988**, *44*, 116.

(38) Carabineiro, H. Ph.D. Thesis, Universidade Técnica de Lisboa and Université Pierre et Marie Curie, Lisbon, Portugal, and Paris, France, 2005.

Other common features include similar W–W distances (3.3 \AA), typical of edge-sharing $\{\text{WO}_6\}^{6-}$ octahedra occurring in zirconium isopolytungstates, that are also found over WZ catalysts.³⁸ However, it should be noticed that the W–Zr distance found in zirconium isopolytungstates (e.g., 3.45 \AA in anion **1b**) is longer than the one found on WZ catalysts (3.14 \AA).³⁸ Therefore, although it is tempting to establish a link between the structure of the monomeric zirconium isopolytungstates and the WO_x phase in WZ catalysts, some structural differences subsist. Nevertheless, the zirconium-containing isopolytungstates presented here allow one to gain further insight into the chemistry of Zr–W mixed compounds and provide useful spectroscopic standards for the study of WZ catalysts.

4. Conclusion

The synthesis and characterization of a series of zirconium-substituted isopolytungstates are described. Single-crystal XRD together with Zr K-edge EXAFS analysis reveals that these compounds are based on $\{\text{W}_5\text{O}_{18}\text{Zr}\}^{2-}$ units derived from the Lindqvist-type hexatungstate $[\text{W}_6\text{O}_{19}]^{2-}$ by formal replacement of a $\{\text{W}^{\text{VI}}=\text{O}\}^{4+}$ fragment by a $\{\text{Zr}^{\text{IV}}(\text{H}_2\text{O})_{3-n}(\text{DMSO})_n\}^{4+}$ group for monomers or $\{\text{Zr}^{\text{IV}}(\mu\text{-OH})\}^{3+}$ for the dimer. The coupling of complementary spectroscopic techniques such as EXAFS, EPR, and vibrational spectroscopies is used to probe the structure of zirconium-containing POMs. Because of different coordinations of the Zr atom in all of these complexes, this extensive spectroscopic characterization provides useful standards for the study of heterogeneous tungstated zirconia catalysts, which appear to be interesting for the skeletal isomerization of light *n*-alkanes.

Acknowledgment. H.C. acknowledges the Portuguese FCT/MCTES Foundation for a Ph.D grant (BD 6855/2001). Financial support from a joint French–Portuguese research project (CNRS-GRICES n. 14149) is also gratefully acknowledged. Beamline time at Elettra was supported by the European Community–Research Infrastructure Action under the FP6 “Structuring the European Research Area” Program (through the Integrated Infrastructure Initiative “Integrating Activity on Synchrotron and Free Electron Laser Science”). The authors are grateful to Bernard Morin for recording the EPR spectra, René Thouvenot for ^{183}W NMR measurements, and Françoise Villain for valuable discussion and help with the EXAFS experiments.

Supporting Information Available: Crystallographic CIF files for compounds $(\text{Me}_4\text{N})_2(\mathbf{1b})\cdot\text{DMSO}\cdot\text{H}_2\text{O}$ and $(\text{Me}_4\text{N})_2(\mathbf{1c})\cdot\text{DMSO}$. This material is available free of charge via the Internet at <http://pubs.acs.org>.

IC051941L